Ultramicroscopy 188 (2018) 41–47

Contents lists available at ScienceDirect

Ultramicroscopy

journal homepage: www.elsevier.com/locate/ultramic

Imaging and electron energy-loss spectroscopy using single nanosecond electron pulses

Matthieu Picher[a,1], Kerstin Bücker[a,1], Thomas LaGrange[b], Florian Banhart[a,*]

[a] Université de Strasbourg, CNRS, Institut de Physique et Chimie des Matériaux, UMR 7504, Strasbourg 67034, France
[b] Interdisciplinary Centre for Electron Microscopy (CIME), École Polytechnique Fédérale de Lausanne (EPFL), Lausanne 1015, Switzerland

ARTICLE INFO

Article history:
Received 25 October 2017
Revised 27 February 2018
Accepted 2 March 2018
Available online 13 March 2018

ABSTRACT

We implement a parametric study with single electron pulses having a 7 ns duration to find the optimal conditions for imaging, diffraction, and electron energy-loss spectroscopy (EELS) in the single-shot approach. Photoelectron pulses are generated by illuminating a flat tantalum cathode with 213 nm nanosecond laser pulses in a 200 kV transmission electron microscope (TEM) with thermionic gun and Wehnelt electrode. For the first time, an EEL spectrometer is used to measure the energy distribution of single nanosecond electron pulses which is crucial for understanding the ideal imaging conditions of the single-shot approach. By varying the laser power, the Wehnelt bias, and the condenser lens settings, the optimum TEM operation conditions for the single-shot approach are revealed. Due to space charge and the Boersch effect, the energy width of the pulses under maximized emission conditions is far too high for imaging or spectroscopy. However, by using the Wehnelt electrode as an energy filter, the energy width of the pulses can be reduced to 2 eV, though at the expense of intensity. The first EEL spectra taken with nanosecond electron pulses are shown in this study. With 7 ns pulses, an image resolution of 25 nm is attained. It is shown how the spherical and chromatic aberrations of the objective lens as well as shot noise limit the resolution. We summarize by giving perspectives for improving the single-shot time-resolved approach by using aberration correction.

© 2018 Elsevier B.V. All rights reserved.

1. Introduction

Most transformations at the nanoscale evolve quickly at high temperatures, stresses, and other external stimuli, which can kinetically drive non-equilibrium states. It is these materials states that are of particular interest. Their study allows fundamental property-structure correlations to be made that are useful for understanding a material's macroscopic behavior in applications. However, observing these non-equilibrium states under rapid microstructural evolution is challenging with conventional microscopy instrumentation, as much of the salient features of the microstructural evolution are missed due to slow recording rates. Laser-based time-resolved transmission electron microscopy (TEM) technologies, working with ultrashort electron pulses instead of continuous beams, aim to improve the temporal resolution of *in-situ* techniques [1,2]. High-temporal resolution is achieved by the synchronization of the laser pump pulse on the samples that initiates materials dynamics with the arrival of the laser-induced photoelectron pulse that probes the dynamics occurring in the material.

The transformation of nanomaterials after an external stimulus can be reversible or irreversible. Correspondingly, there are two approaches implemented in the laser-based TEM technologies, stroboscopic [2–6] and single-shot [1,7–11], which are complementary in their parametric ranges. These time-resolved TEM techniques overcome the signal limitations of conventional electron sources by using laser-induced electron emission, producing much higher peak currents within the pulse (e.g., μA to tens of mA). Such intense beams come at a cost; electrons are closer in space and scatter off each other (Coulomb interaction) [12] that degrades the resolution of the time-resolved electron microscopy techniques. The stroboscopic method minimizes Coulomb effects by limiting the number of electrons in the probe pulse, requiring integration of millions of pump-probe events to build-up enough signal for an image or diffraction pattern. Though the stroboscopic approach under specific conditions provides femtosecond time resolution and sub-nanometer spatial resolution [5,6,13], the materials processes that it can usefully interrogate must be fully reversible. However, due to inevitable entropy increase, the majority of the material processes of interest in chemistry and materials science

* Corresponding author.
E-mail address: florian.banhart@ipcms.unistra.fr (F. Banhart).
[1] These authors have contributed equally to this work.

https://doi.org/10.1016/j.ultramic.2018.03.006
0304-3991/© 2018 Elsevier B.V. All rights reserved.

tend to be irreversible, e.g., first-order phase transitions or irreversible chemical and structural changes, requiring the use of the single-shot approach to study their ultrafast materials dynamics.

The single-shot approach explores nonrepetitive events by taking "snap-shot" images using electron pulses with a bunch length of 5 ns to hundreds of nanoseconds that contain up to billions of electrons [11,14]. With such high amount of electrons in a single pulse, the Boersch effect, lateral space-charge effects, and trajectory displacements pose significant challenges for imaging and spectroscopy using these intense electron pulses [8,12,15,16]. In the nanosecond regime, Coulomb repulsion and Boersch effects have a negligible influence on the temporal resolution, slightly increasing the pulse duration by a couple of nanoseconds [15,17,18]. However, Boersch effects dramatically increase the energy spread and the lateral extension of the pulse, requiring trade-offs to be made in signal and spatial coherence. Though prior work has described, theoretically and through simulations, the influence of Coulomb interactions and has given perspectives on the resolution limits [8,12,15,16], no direct correlation or systematic experimental study has been made about the impact of microscope and laser parameters on the resolution of the single-shot approach.

Here, we explore the influence of pulse electron current, Wehnelt bias, and the convergence angle of the probe on the spatial resolution of single-shot images as well as on the energy resolution in EELS and quantify their effect on the resolution. Due to a large number of electrons needed for imaging in the single-shot approach, Boersch effects and large energy spreads are an inherent and unavoidable consequence. However, electrons within a narrow range of kinetic energy can be selected using an appropriate configuration of the Wehnelt electrode to obtain energy filtering so that enough temporal and spatial coherence is achieved for imaging. A similar method has been used in the stroboscopic approach to increase pulsed electron beam coherence, which was termed chromatic filtering [6], though at the cost of signal. Increasing the signal in the single-shot approach can be accomplished by lengthening the pulse duration, which requires complex and large laser systems [11]. At a fixed laser pulse duration, increasing signal can only be achieved by making a trade-off between the use of converged beams and increased aberrations. Thus, we aim to find the optimal resolution for both imaging and diffraction by experimentally quantifying shot noise limits and the influence of spherical and chromatic aberration on spatial resolution.

Exploring the influence of electron optical and laser parameters also allows us to define suitable conditions for performing core-loss electron energy-loss spectroscopy. In this article, we show the first electron energy-loss spectra recorded with single nanosecond electron pulses. In comparison to conventional core-loss EELS spectra, which are rarely acquired with exposure times below a few milliseconds, the single-shot DTEM technique can provide six orders of magnitude in temporal resolution, though at the expense of energy resolution and counting statistics. Nonetheless, under particular electron optical and laser conditions core-loss EELS spectroscopy can be performed at acquisition times of less than 10 ns.

2. Experimental methods

The experiments were carried out by using a Jeol 2100 with thermionic gun setup including a Wehnelt electrode. The setup is shown schematically in Fig. 1. The microscope was modified by IDES Inc. to serve for ultrafast imaging [4,6]. An additional condenser lens CL_0 above the CL_1 lens allows increased collection of electrons and the focusing of the electron beam through a hole in a molybdenum mirror that is located between the condenser lenses CL0 and CL1 and reflects the UV laser beam onto the photocathode. The optical tables housing the lasers with the optical setup were attached to the column. As emitter, a Ta disc (0.8 mm diameter) was used. The Wehnelt bias was adjustable within a range of 83–1125 V. All experiments were performed at 200 kV acceleration voltage of the microscope. For creating photoelectron pulses, a nanosecond laser (Litron Nano T) emitting UV pulses (213 nm) with a duration of 7 ns at an energy of up to 0.4 mJ per pulse was used either in the single-pulse mode or at a repetition frequency of 20 Hz. In the pump-probe approach, a femtosecond fiber laser (Amplitude Satsuma) was used for inducing transformations in the sample. An EEL spectrometer (Gatan Enfinium) was used for spectroscopy.

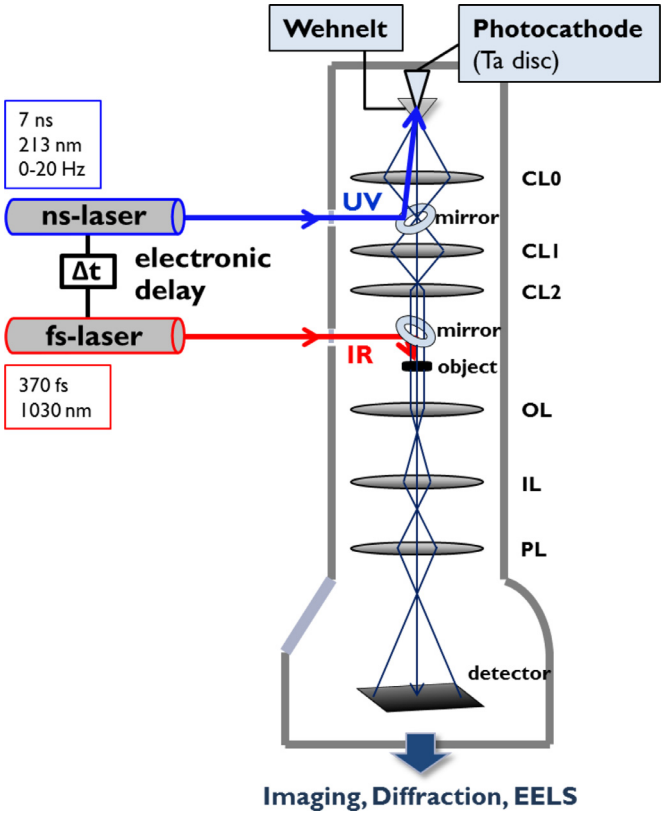

Fig. 1. Schematic drawing of the single-shot UTEM setup. The electron-optical setup and ray paths are simplified (not all lenses are shown).

A detailed characterization of the nanosecond electron pulses was accomplished by varying the UV laser power (that determines the number of electrons per pulse) and the Wehnelt bias. The influence of both parameters on the electron pulse energy spread and the image resolution was studied. The temporal resolution of the microscope is mainly limited by the duration of the nanosecond laser pulses; the electron-optical parameters only have an influence up to an order of 100 ps [6] and are therefore negligible in this setup. The influence of other parameters such as the cathode-Wehnelt distance, the current in the C_0 lens, or the beam convergence angle at the specimen were also studied.

The number of electrons per pulse is the decisive parameter in single-shot imaging and was estimated according to the following procedure. For improved accuracy, the energy of the UV pulses arriving on the photocathode was measured with the electron gun removed. The reflectivity of the Ta cathode is ~70%, and the conversion efficiency at 213 nm is 10^{-4} [19]. For a typical UV pulse energy of 565 µJ, which is at the upper end of the energies used in this study, we obtain approximately 9×10^9 electrons per pulse. However, a certain fraction of the photoelectrons is lost in the Wehnelt, on the anodes, and on the different apertures in the column. The transmission through the column depends on the

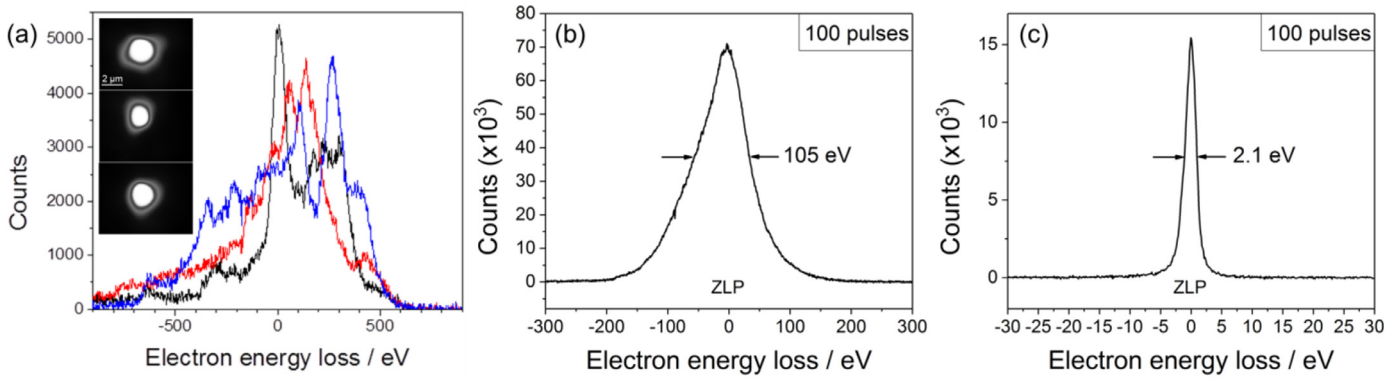

Fig. 2. The Zero-loss peak of EEL spectra taken with electron pulses of 7 ns. (a): Comparison of three single pulses (black, red, and blue spectrum) taken at a UV laser pulse energy of 85 µJ and minimum Wehnelt bias. Inset: grey-scale electron beam profile for three different shots (not the same as the spectra) with a fully focused spot. (b): EELS at Wehnelt bias of 80 V; (c): EELS at Wehnelt bias of 1000 V; both at low intensity of UV pulses (5 µJ). Both spectra are averaged over 100 pulses to facilitate the measurement of the width. (For interpretation of the references to color in this figure legend, the reader is referred to the web version of this article.)

Wehnelt bias, the lens currents, and the diaphragms. At 565 µJ UV pulse energy and all apertures retracted for maximum transmission, an average current of 800 pA is measured on the fluorescent screen at a repetition frequency of 20 Hz, corresponding to 2.5×10^8 electrons per pulse. The same order of magnitude is obtained by acquiring the pulses with the CCD camera. Thus, approximately 98% of the photo-emitted electrons are lost between the cathode and the screen or detector in the present configuration, i.e., with all parameters optimized for maximizing electron transmission through the column. In a standard TEM, i.e., without C_0 lens, the loss would be even higher.

3. Results

3.1. Energy width of nanosecond electron pulses

The energy width of the pulses is not only of importance in EELS but also for imaging due to the considerable influence of the chromatic aberration of the objective lens on the image at high energy spreads. The energy spread is measured as the full width at half maximum of the zero-loss peak (ZLP). EEL spectra were taken in the imaging or diffraction mode where as many electrons as possible are focused through the entrance aperture (2 mm) of the spectrometer. It is found that the width of the ZLP depends on the energy of the laser pulses as well as on the Wehnelt bias.

Fig. 2(a) shows EEL spectra and the appearance of the focused electron spot (image taken from the spot without specimen) under the conditions of the minimum Wehnelt bias voltage setting. It is apparent that three individual pulses result in quite different spectra and electron beam profiles. This is due to unavoidable instabilities in the operation of the flashlamp-pumped nanosecond laser with 5th harmonic generation. Energy widths of the order 500 eV are obtained which are unsuitable for EELS and imaging. Fig. 2(b) shows the peak for low Wehnelt bias and a lower laser pulse energy. The energy width is still around 100 eV under these conditions. However, the situation improves drastically when the Wehnelt bias is increased. Fig. 2(c) shows the zero-loss peak at maximum bias and a UV energy of 5 µJ/pulse. The spectra were integrated over 100 pulses to eliminate noise. An energy width of 2.1 eV can be obtained, though at considerable expense of counts in the spectrum.

Fig. 3 shows ionization edges taken with one single 7 ns pulse. The carbon K edge in Fig. 3(a) was taken from carbon nanotubes. At an energy width of 30 eV in this case, the fine structure of the spectrum is not visible, but the presence of carbon can be clearly shown. Fig. 3(b) shows the oxygen K and the nickel L edge taken from a nickel oxide film with a 7 ns pulse at an energy width of 60 eV. Energy widths of 30 or 60 eV seem high in comparison to conventional TEM; however, ionization edges can be clearly identified and separated if they are not too close to each other, and the presence of the respective elements can be shown. Even a rough quantitative estimation of the composition seems feasible.

Fig. 4 shows the influence of the Wehnelt bias on the energy width and the number of electrons in the pulses at different laser pulse energies. A comprehensive study at different laser pulse energies is shown in Fig. 4(a). To obtain the curves, the Wehnelt bias was increased from the top right to the bottom of the data points. A turning point appears at high bias and low ΔE. This is due to the appearance of the halo in the emission pattern close to saturation [6] which focuses a population of off-axis electrons into the beam spot. In the bottom half of the curves, below the turning point, the halo contributes, causing an observable increase in the energy width. To achieve low energy spread, the optimum operation conditions are therefore close to the turning point on the left-hand side in Fig. 4(a). As a detail from Fig. 4(a) at a UV pulse energy of 85 µJ, Fig. 4(b) shows the decreasing energy width and number of electrons with increasing bias. Generally, a reasonable compromise between energy width and counting statistics can be found.

3.2. Imaging with nanosecond pulses

As in EELS studies, the critical parameters in the single-shot operation are the number of electrons per pulse and the energy width of the pulses. Whereas noise generally leads to a limit of information in an image, increased energy width degrades the image resolution due to the chromatic aberration of the objective lens. Furthermore, since the pulses have low intensity, the beam must be focused onto the specimen which also degrades the resolution due to the spherical aberration of the objective. These contributions were studied separately by taking the same images with one single pulse as well as with a high number of pulses. The latter eliminates the contribution of shot noise so that aberration effects can be studied separately. Pulse lengths of 7 ns were used for all imaging studies.

We first study the influence of the energy width on the resolution. Fig. 5 shows images of gold nanoparticles on an amorphous carbon film at different Wehnelt bias settings. To eliminate the influence of image noise, all images have been recorded at a constant signal intensity by integrating over a certain number of pulses. The series has been taken at a UV pulse energy of 400 µJ which is close to the upper limit. It is clearly visible how the image resolution im-

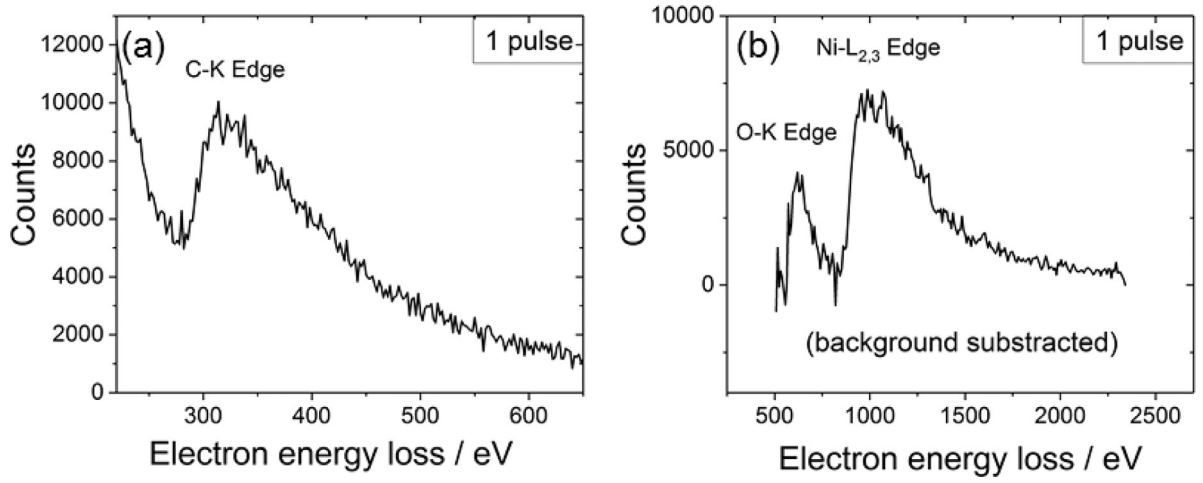

Fig. 3. Single-shot EEL spectra of absorption edges taken with single electron pulses of 7 ns. (a) Single-shot carbon K-edge of carbon nanotubes, with $\Delta E = 30$ eV, 5×10^6 e/pulse (bias = 665 V, UV pulse energy 200 µJ). (b) Single-shot spectrum obtained from a 40 nm thick NiO calibration sample showing the oxygen K-edge and the nickel L-edge at $\Delta E = 60$ eV and 5×10^7 e/pulse (bias = 560 V, UV pulse energy 450 µJ).

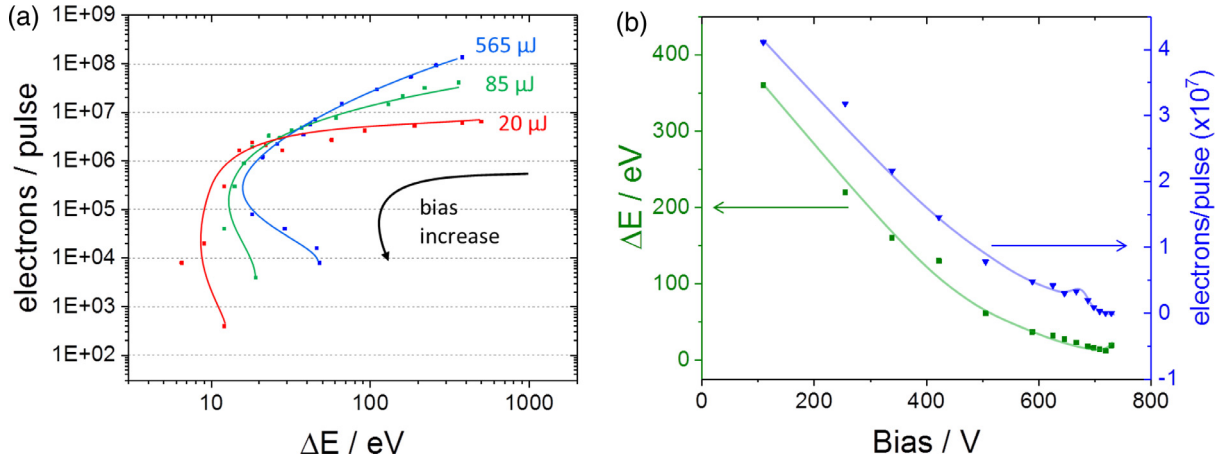

Fig. 4. (a) Number of electrons per pulse as a function of energy spread for different laser pulse energies at a cathode-Wehnelt gap of 630 µm. The Wehnelt bias increases along the curves from top right to the bottom. (b): Energy spread and number of electrons per pulse as a function of Wehnelt bias at laser pulses of 85 µJ.

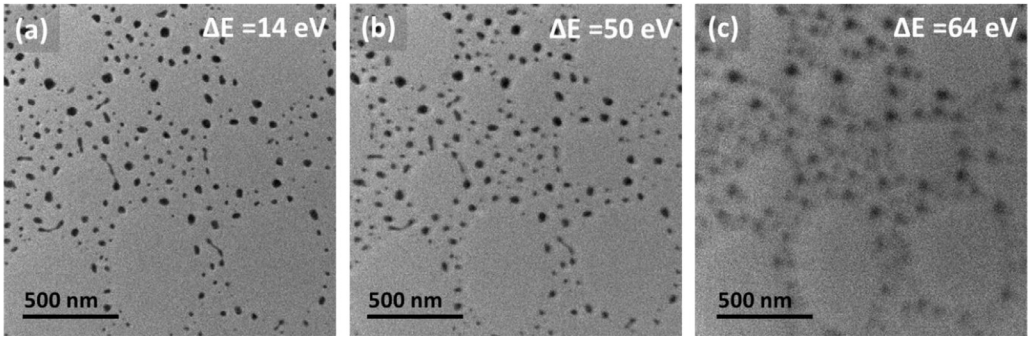

Fig. 5. Gold particles on an amorphous carbon membrane imaged with different bias settings, corresponding to different energy widths of the pulses. Images were taken at constant signal intensity by integration over a different number of pulses. (a) $\Delta E = 14$ eV, 2400 pulses (4×10^5 e/pulse), bias = 790 V, estimated resolution = 5 nm. (b) $\Delta E = 49$ eV, 600 pulses (1.7×10^6 e/pulse), bias = 600 V, resolution = 13 nm. (c) $\Delta E = 64$ eV, 400 pulses (2.5×10^6 e/pulse) bias = 520 V, resolution = 28 nm. The laser pulse energy was 400 µJ.

proves with increasing bias and decreasing energy width although the lens currents of the microscope remain unchanged. The image resolution was estimated by measuring the width of the blurred edges of larger particles that give enough contrast (at perfect resolution, the edges would appear sharp at moderate magnification). While the resolution is 28 nm in the low-bias regime, a resolution down to 5 nm is achieved at high bias. It is obvious that the chromatic aberration of the objective leads to a blurring of the image due to the higher energy spread. With the chromatic aberration coefficient $C_c = 1.4$ mm of the objective and an illumination semi-angle $\alpha = 33$ mrad (determined by measuring the diameter of the central spot in a convergent beam electron diffraction pattern), we can estimate the chromatic resolution limit $r_{chr} = C_c \alpha \Delta E/E$ of 15 nm at $\Delta E = 64$ eV and 3.2 nm at 14 eV. The calculated resolution r_{chr} is

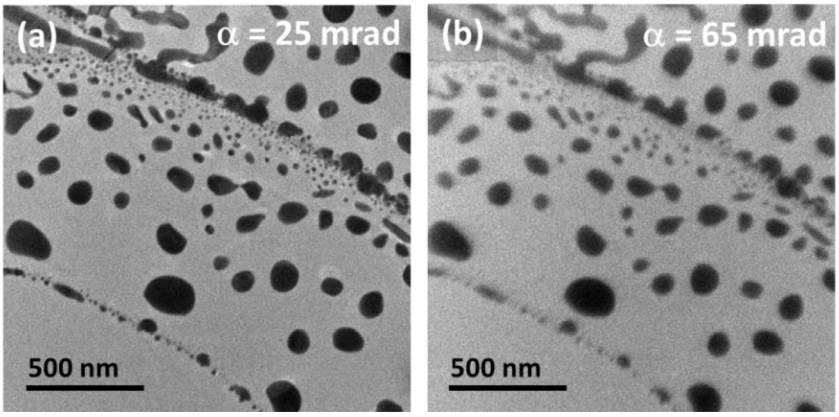

Fig. 6. Images of gold particles recorded with different convergence angles of the beam and taken at constant signal intensity (UV pulse energy 400 µJ, bias = 750 V, ΔE = 22 eV, i.e. 10^9 electrons in each image). (a) $\alpha = 25$ mrad, 8000 pulses, image resolution = 5 nm. (b) $\alpha = 65$ mrad, 100 pulses, resolution = 25 nm.

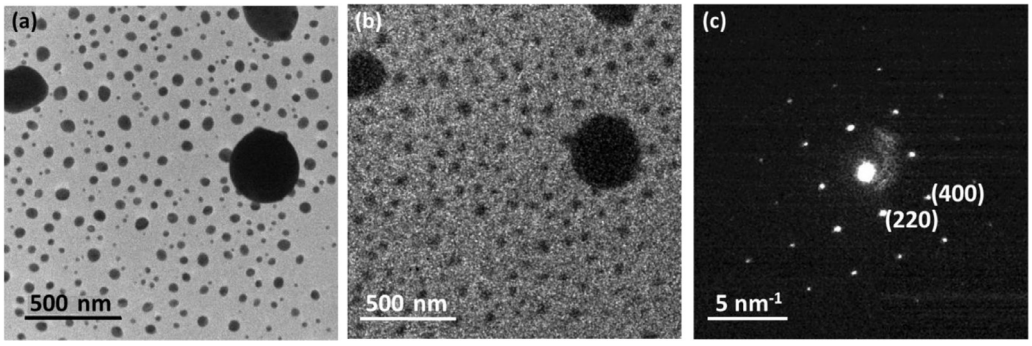

Fig. 7. Comparison of a 1000-pulse image (a) with a single-pulse image (b). Pulse duration: 7 ns. Convergence angles $\alpha = 25$ mrad (a) and $\alpha = 45$ mrad (b) were used. The energy widths were ΔE = 25 eV (a) and ΔE = 35 eV (b) corresponding to bias settings of 720 V and 670 V, respectively. (c) Single-shot diffraction pattern obtained from a Si monocrystal in the (100) zone axis orientation, with ΔE = 43 eV and almost parallel illumination (2×10^5 electrons).

about half the measured values, suggesting that other factors, like spherical aberration, play a role.

Since the overall number of electrons is low in single-shot imaging, working with a parallel electron beam does not lead, in most cases, to a sufficient number of electrons on the camera. This, again, limits the visibility of the specimen features of interest. The beam has to be converged to a high illumination angle, leading to increased influence of spherical aberration. Although it is well-known how the convergence angle influences spatial resolution in conventional TEM, it was studied here for nanosecond pulses. Fig. 6 shows two examples for convergence angles of 25 and 65 mrad. Correspondingly, the number of electrons reaching the camera differs by an order of magnitude. The blurring is obvious in the image taken with a converged beam; the resolution is approximately 25 nm, compared to 5 nm with the expanded beam. A comparison with the expected values, based on a rough estimation with the spherical aberration coefficient of $C_s = 1.0$ mm and the resolution limit of $r_{sph} = 0.25 C_s \alpha^3$, leads to a resolution of 68 nm for a convergence angle of 65 mrad and 3.9 nm for 25 mrad. This low angle value is roughly in agreement with the experimental resolution (5 nm). However, the estimation is difficult for large angles due to the third power relation between angle and resolution.

An important limitation in single-shot imaging is the low signal/noise ratio. The influence of noise was studied by comparing multi-pulse with single-pulse images taken under optimized conditions for each case. Fig. 7(a) and (b) show the difference between a 1000-pulse and a single-pulse image taken from the same specimen. Noise in the single-shot image is considerable and limits the resolution. No noise filtering was applied. The measured step edge resolution is 25 nm in the single-shot image, while a resolution down to 3 nm can be achieved with many pulses under optimum conditions (low energy spread, low convergence angle).

3.3. Nanosecond electron diffraction

The parameters limiting EELS and imaging, namely energy spread, aberrations, and noise, have an influence on diffraction patterns, though in a different way than in imaging. Diffraction disks instead of pin-point spots appear in the back focal plane when convergent illumination is used. Even for a parallel beam, the spots are broadened due to the large virtual source size and low spatial coherence of the beam (disk-shaped cathode, C_0 lens, and large condenser aperture). At low Wehnelt bias, the gun cross-over remains unfiltered in energy and space and appears large. Furthermore, the diffraction spots are widened due to the contribution of electrons with different energy and the chromatic aberrations of the condenser and the objective (although this is a minor effect). Due to the contribution of the convergence angle to the chromatic aberration, the influence of chromatic aberration can be reduced by using smaller condenser apertures. In each case, it is mandatory to work under high-bias conditions, which reduces the energy width as well as the virtual source size. Noise has less influence on diffraction than on imaging due to the concentration of all electrons into the diffraction spots. Broadening of the spots due to variations of the Bragg angle at high energy spread is approximately three orders of magnitude smaller than the diameter of the diffraction disk, even at ΔE = 100 eV, and therefore negligible. An example of a single-shot diffraction pattern taken with optimized settings is shown in Fig. 7c.

4. Discussion

Previous studies have already considered the influence of some beam parameters on single-shot imaging [8,12,15]. However, since EELS has not been available in the previously used instrument, the energy distribution of the pulses remained unknown. Now, with our knowledge about the energy distribution and the possibility to reduce the energy width of the pulses by adjusting the Wehnelt bias, a more comprehensive understanding on what limits resolution can be obtained. We discuss the requirements for imaging and EELS which are different in that high spatial resolution and coherence are required for imaging but not for EELS.

4.1. Imaging

Due to repulsion effects in the lens cross-overs, random scattering of electron trajectories in the back focal plane of the objective can blur the imge and reduce spatial resolution. These effects in the objective are thought to be the ultimate limit for single-shot imaging as it has been predicted earlier [8]. However, the present study shows that this limit is not reached under realistic operation conditions. As shown experimentally, the resolution is limited by a combination of chromatic aberration, spherical aberration, and shot noise. Coulomb interactions at the cathode and Wehnelt crossover are severe. Applying a high bias to the Wehnelt cap, e.g., >400 V, allows monochromation of the beam and reduces the energy spread of the intense electrons pulses to a range of 30–70 eV, which is still acceptable for imaging with a resolution of some nanometers. Use of a monochromatior greatly reduces the pulse electron current, increases noise and requires the use of converged beams that increase aberrations. Furthermore, it has to be taken into account that the spatial coherence length within the pulses is very low, most likely of the order of nanometers, due to the large virtual source size in the single-shot setup. The additional condenser lens C_0 and the fully retracted condenser aperture increase signal but reduce coherence.

Depending on the system studied with single pulses, a balance between two opposing conditions, reduced energy spread and the required signal on the detector, has to be found to obtain the optimal resolution. For reaching an acceptable noise level, i.e., to be above the shot-noise-limited resolution, the number of counts on each pixel of the camera has to be as high as possible. This can be achieved by increasing the UV power and/or decreasing the Wehnelt bias to obtain intense electron pulses. On the other hand, the number of electrons per pulse has to be kept small to reduce the energy width and the influence of chromatic aberrations.

According to the Rose criterion [20], the shot noise in an image has to be smaller than the contrast divided by the number of gray scale levels [8,16]. The shot noise is defined as $N^{-1/2}$ where N is the number of counts per pixel. If we assume a minimum useful contrast of 0.5 and 5 necessary gray levels, we obtain a shot noise of 0.1 and, accordingly, 100 counts per pixel. In the example of the single-shot image (Fig. 7(b)), 10^6 electrons contributed to the image formation which would allow an exposure on 10^4 pixels by 100 electrons on each pixel or an image of approximately 100×100 pixels. The typical illuminated specimen area has a size of 1.7 µm× 1.7 µm, hence 1.7 µm/100 pixel yields $r_{SN} = 17$ nm/pixel. However, under the conditions of this study, a resolution of 17 nm is slightly below the achieved resolution. This shows that the influence of aberrations is important. The energy spread of $\Delta E = 35$ eV and $\alpha = 45$ mrad yield resolution limits of $r_{chr} = 11$ nm and $r_{sph} = 23$ nm. As total resolution limit calculated by $\sqrt{r_{SN}^2 + r_{chr}^2 + r_{sph}^2}$ we obtain 31 nm, which is slightly larger than the limit of 25 nm as estimated from the images. As we see from the quantitative estimations in the previous section based on the chromatic and spherical aberration of the objective, the resolution is limited by the unavoidable energy spread and beam convergence. Hence, a certain balance between noise and aberrations can be obtained to reach the resolution limit under the given operation conditions. The best image resolution of 25 nm in this study is achieved at a UV power of 400 µJ/pulse, a Wehnelt bias of 670 V, and a beam convergence angle of 45 mrad. This turned out to be a useful compromise between aberration and noise limits.

4.2. EELS

To obtain a useful EEL spectrum that provides interpretable information, a sufficient number of electrons per pulse and an acceptable energy spread are required to observe the desired features of the ionization edges. The diameter of the fully focused spot on the specimen and the entrance aperture of the spectrometer limit the lateral selectivity and define the spatial resolution. It is obvious that the operation with low Wehnelt bias is unsuitable for EELS due to both the high energy width of the pulses and low spatial resolution (large spot size). In conventional TEM instruments, the maximum energy spread, being largest for thermionic guns, is less than 2 eV. This allows the analysis of fine structures within the edges, requiring at least 2–3 eV. Although low energy spreads can, in principle, be attained in zero-loss peaks using nanosecond pulses (Fig. 2(b)), the need of signal in high-loss EELS of the ionization edges pushes the limits towards 30–60 eV (Fig. 3). Nevertheless, the ionization edges of carbon, oxygen and nickel are clearly visible at such energy spreads of tens of eV. High-energy spreads pose difficulties for detecting the fine structure of the edges and precise quantification. However, in many experiments, detecting the presence and observing relative changes in composition during rapid nanomaterial dynamics would already provide tremendous insights. For example, the rapid decomposition of unstable particles under heating or the explosive release of gases can now be studied at high temporal resolution. Under high temperatures in combination with the high surface area to volume ratio and the small particle diameters make mass transport and reaction rates fast, requiring nanosecond time resolution to elucidate their dynamics. Furthermore, the experimental configuration of the present UTEM allows flexibility in tuning the EELS parameters for given experiments. For example, in the high-bias regime, we are able to work with low energy widths at the expense of signal, but this would allow applications in the low-loss regime of the spectrum. Also, the UV laser power can be reduced that again reduces the energy spread. Increasing the Wehnelt-filament gap also provides higher temporal coherence but again decreases the beam current. The balance between noise in the spectrum and energy resolution has to be adjusted to detect the desired features in the EEL spectrum. Since the diameter of the focused beam is relatively large, the analysis of smaller features of the specimen is difficult. Objects that are much smaller than the beam diameter such as isolated nanoparticles receive only a small fraction of the electrons within a pulse and contribute with a low signal to the spectrum. The lateral selectivity of EELS in the single-shot operation is therefore limited due to the large beam diameter. In spite of these limitations, quantitative ultrafast EELS studies can now be launched.

5. Conclusions and perspectives

The first application of an EEL spectrometer in a single-shot, nanosecond time-resolved TEM shows that the energy width of the nanosecond electron pulses is a crucial parameter. Not only sets the energy resolution the limits for EELS, it also has a considerable influence on the image resolution due to the chromatic aberration of the objective. The necessity of converging the beam onto the specimen due to the low number of electrons in one pulse imposes

a considerable influence of the spherical aberration on the imaging. Finally, shot noise in the weak electron pulses necessitates the collection of as many electrons as possible from a large angular range and requires the use of a moderate Wehnelt bias that produces pulses with large energy widths.

Since EELS has already been carried out in stroboscopic UTEMs since some time [21,22], a long-lasting question, namely whether EELS can principally be carried out in single-shot TEM, can now be answered positively. Although the fine structure of the edges might only be resolvable in a few cases, the ionization edges in an energy range up to certainly more than 1000 eV can be easily detected so that the dynamics of fast irreversible chemical reactions can now be studied at high spatial and temporal resolution.

An improvement of the spatial resolution necessitates an extensive instrumental development. Due to the repulsion and scattering of electrons near the cathode, the single shot approach is inherently signal-limited. High energy spreads due to the Boersch effect in the gun and the resulting chromatic aberration can only be reduced in the current instrument designs by using the Wehnelt as a crude monochromator. This greatly reduces the signal and increases noise in the image. The implementation of C_c and C_s correctors (after the objective lens) would allow the use of large energy widths and high illumination angles. This would allow us to reach the noise limit. As the above-mentioned estimation shows, a resolution down to approximately 2–3 nm, hence a gain of one order of magnitude, could be achievable in the single-shot mode. Since shot noise would still limit the resolution after correction of aberrations, a camera with higher detection efficiency such as a direct detection CMOS camera would be another advantage. This has already been realized in a recent study on a dynamic TEM [13]. On the level of the gun, an improved design of the Wehnelt electrode could reduce space charge and allow pulses of lower energy width. If the gun cross-over can be shifted to higher electron energies within the acceleration regime, this would reduce the Boersch effect in the cross-over. The Wehnelt with its chromatic aberration is used in the present configuration as a monochromator, allowing us to reduce the energy width of the pulses. This could be improved by using a dedicated monochromator in the gun with better control over the energy width.

Acknowledgment

Funding by the EQUIPEX program of the Agence Nationale de Recherche (France), contract ANR-11-EQPX-0041 (project UTEM) is gratefully acknowledged.

References

[1] W.E. King, G.H. Campbell, A. Frank, B. Reed, J.F. Schmerge, B.J. Siwick, B.C. Stuart, P.M. Weber, Ultrafast electron microscopy in materials science, biology, and chemistry, J. Appl. Phys 97 (2005) 111101.
[2] A. Zewail, Four-dimensional electron microscopy, Science 328 (2010) 187–193.
[3] V.A. Lobastov, R. Srinivasan, A. Zewail, Four-dimensional ultrafast electron microscopy, Proc. Natl. Acad. Sci. USA 102 (2005) 7069–7073.
[4] L. Piazza, D.J. Masiel, T. LaGrange, B.W. Reed, B. Barwick, F. Carbone, Design and implementation of a fs-resolved transmission electron microscope based on thermionic gun technology, Chem. Phys. 423 (2013) 79–84.
[5] A. Feist, K.E. Echternkamp, J. Schauss, S.V. Yalunin, S. Schäfer, C. Ropers, Quantum coherent optical phase modulation in an ultrafast transmission electron microscope, Nature 521 (2015) 200–203.
[6] K. Bücker, M. Picher, O. Crégut, T. LaGrange, B.W. Reed, S.T. Park, D.J. Masiel, F. Banhart, Electron beam dynamics in an ultrafast transmission electron microscope with wehnelt electrode, Ultramicroscopy 171 (2016) 8–18.
[7] T. LaGrange, M.R. Armstrong, K. Boyden, C.G. Brown, G.H. Campbell, J.D. Colvin, W.J. DeHope, A.M. Frank, D.J. Gibson, F.V. Hartemann, J.S. Kim, W.E. King, B.J. Pyke, B.W. Reed, M.D. Shirk, R.M. Shuttlesworth, B.C. Stuart, B.R. Torralva, Single-shot dynamic transmission electron microscopy, Appl. Phys. Lett. 89 (2006) 044105.
[8] M.R. Armstrong, K. Boyden, N.D. Browning, G.H. Campbell, J.D. Colvin, W.J. DeHope, A.M. Frank, D.J. Gibson, F. Hartemann, J.S. Kim, W.E. King, T.B. LaGrange, B.J. Pyke, B.W. Reed, R.M. Shuttlesworth, B.C. Stuart, B.R. Torralv, Practical considerations for high spatial and temporal resolution dynamic transmission electron microscopy, Ultramicroscopy 107 (2007) 356–367.
[9] J.S. Kim, T. LaGrange, B.W. Reed, M.L. Taheri, M.R. Armstrong, W.E. King, N.D. Browning, G.H. Campbell, Imaging of transient structures using nanosecond in situ TEM, Science 321 (2008) 1472–1475.
[10] T. LaGrange, G.H. Campbell, B.W. Reed, M. Taheri, J.B. Pesavento, J.S. Kim, N.D. Browning, Nanosecond time-resolved investigations using the in situ of dynamic transmission electron microscope (DTEM), Ultramicroscopy 108 (2008) 1441–1449.
[11] T. LaGrange, B.W. Reed, D.J. Masiel, Movie-mode dynamic electron microscopy, MRS Bull. 40 (2015) 22–28.
[12] B.W. Reed, M.R. Armstrong, N.D. Browning, G.H. Campbell, J.E. Evans, T. LaGrange, D.J. Masiel, The evolution of ultrafast electron microscope instrumentation, Microsc. Microanal. 15 (2009) 272–281.
[13] Y.M. Lee, Y. J.Kim, Y.-J. Kim, O.-H. Kwon, Ultrafast electron microscopy integrated with a direct electron detection camera, Struct. Dyn. 4 (2017) 044023.
[14] T. LaGrange, B.W. Reed, M.K. Santala, J.T. McKeown, A. Kulovits, J.M.K. Wiezorek, L. Nikolova, F. Rosei, B.J. Siwick, G.H. Campbell, Approaches for ultrafast imaging of transient materials processes in the transmission electron microscope, Micron 43 (2012) 1108–1120.
[15] B.W. Reed, Femtosecond electron pulse propagation for ultrafast electron diffraction, J. Appl. Phys. 100 (2006) 034916.
[16] M.R. Armstrong, B.W. Reed, B.R. Torralva, N. Browning, Prospects for electron imaging with ultrafast time resolution, Appl. Phys. Lett. 90 (2007) 114101.
[17] B.J. Siwick, J.R. Dwyer, R.E. Jordan, R.J.D. Miller, Ultrafast electron optics: Propagation dynamics of femtosecond electron packets, J. Appl. Phys. 92 (2002) 1643–1648.
[18] S.T. Park, O.H. Kwon, A.H. Zewail, Chirped imaging pulses in four-dimensional electron microscopy: femtosecond pulsed hole burning, New J. Phys. 14 (2012) 053046.
[19] T. Anderson, I.V. Tomov, P.M. Rentzepis, Laser-driven metal photocathodes for picosecond electron and x-ray pulse generation, J. Appl. Phys. 71 (1992) 5161–5167.
[20] A. Rose, Television pickup tubes and the problem of vision, Adv. Electron. Electron. Phys. 1 (1948) 131–166.
[21] L. Piazza, C. Ma, H.X. Yang, A. Mann, Y. Zhu, J.Q. Lee, F. Carbone, Ultrafast structural and electronic dynamics of the metallic phase in a layered manganite, Struct. Dyn. 1 (2014) 014501.
[22] R.M. van der Veen, T.J. Penfold, A.H. Zewail, Ultrafast core-loss spectroscopy in four-dimensional electron microscopy, Struct. Dyn. 2 (2015) 024302.